A Lagrangian Central Scheme for Interface Problems

Riccardo Fazio*
Department of Mathematics, University of Messina
Salita Sperone 31, 98166 Messina, Italy
e-mail: rfazio@dipmat.unime.it

Giovanni Russo
Department of Mathematics and Computer Science, University of Catania,
Viale Andrea Doria 6, 95126 Catania, Italy.
e-mail:russo@dmi.unict.it

Abstract

We study high-resolution Lagrangian central schemes for the one-dimensional system of conservation laws describing the evolution of two gases in slab geometry separated by an interface. By using Lagrangian coordinates, the interface is transformed to a fixed coordinate in the computational domain and, as a consequence, the movement of the interface is obtained as a byproduct of the numerical solution. The main contribution is the derivation of a special equation of state to be imposed at the interface in order to avoid non-physical oscillations. Suitable boundary conditions at the piston that guarantee second order convergence are described.

*Corresponding author.

We compare the solution of the piston problem to other results available in the literature and to a reference solution obtained in the adiabatic approximation. A shock-interface interaction problem is also treated. The results on these tests are in good agreement with those obtained by other methods.

Key Words. Lagrangian central schemes, Euler equations, interface conditions, boundary conditions.

AMS Subject Classifications. 65M06, 65M99, 76T05.

Acknowledgment. The research of this work was supported by grants of the Catania and Messina Universities and partially by the Italian "MIUR".

1 Introduction

The numerical simulation of interface and multi-fluid problems is a research topic of relevant interest in several branches of the applied sciences. To mention some issues, we have: bubble evolution in nuclear flows, combustion applications, etc.

We study high-resolution Lagrangian central schemes for the one-dimensional system of conservation laws describing the evolution of two gases in slab geometry separated by an interface. By using Lagrangian coordinates, the interface is transformed to a fixed coordinate in the computational domain and, as a consequence, the movement of the interface is obtained as a byproduct of the numerical solution. The idea to apply a Lagrangian method to interface problems is not new and for a survey on this subject we refer to Benson [4].

The difficulties to retain pressure equilibrium at the interface has been indicated as the main reason for the failure of many successful single component schemes when applied to multi-component problems by several authors (see the review article by Abgrall and Karni [3] and the references quoted therein). A solution to this problem has been to use the pressure equation in the cells near the interface, as proposed by Karni [12] and investigated by Abgrall [2]. In this way the scheme is not entirely conservative, but lack of conservation, that can be checked *a posteriori*, is quite small. A similar approach has been used by Fedkiw *et al.* [9], [10] in the context of multi-fluid flows and by Wang *et al.* [16] within a mass conservation principle. The intrinsic difficulty related to the evolution

of the interface has induced some authors, Davis [5] and Fazio and LeVeque [7] to apply an exact Riemann solver at the interface to find an approximation of its velocity.

Here we propose the use of a central scheme which is conservative and does not require the solution to exact or approximate Riemann problems. Furthermore, by using Lagrangian coordinates, we do not require the use of additional equations for the interface motion, as is done, for example, with level set methods (see Mulder et al. [14]) or mass fraction models (see Abgrall [1] and Larouturou [13]). This scheme is based on the derivation of a suitable equation of state for the pressure to be used in the cell containing the interface. Preliminary work on this subject has been presented to the Magdeburg hyperbolic conference in 2000 [8] and to the 2001 ENUMATH conference [6].

To validate the scheme we perform several tests and compare the results with those obtained by other methods. In particular we consider the piston problem treated by Fazio and LeVeque [7], a reference solution of the equation of motion of the piston in the adiabatic approximation, and a shock-interface interaction problem of Abgrall and Karni [3]. Other numerical tests can be found in the quoted conference proceedings [8] and [6].

A detailed description of the boundary conditions at the piston is provided. The new boundary condition is obtained by applying the piston equation of motion on the boundary, and by the use of the adiabaticity condition at the piston. It is shown that the usual reflecting boundary conditions, although consistent with the governing equations, leads to a degradation of the accuracy.

The plan of the paper is the following. Next section is devoted to the physical description of the problem, and to the equations in Lagrangian coordinates. In section 3 we consider the piston problem for a single gas. After a brief review of the Nessyahu-Tadmor scheme, we describe in detail how to implement second order boundary conditions at the piston. The last part of the section is devoted to numerical tests on a single gas piston problem.

In Section 4 we describe the equation of state for the cell containing the interface. Section 5 contains several numerical tests for two fluid problems, solved by the new scheme and compared with adiabatic limits and solutions obtained by other methods. In the last section we draw some conclusions.

2 Description of the problem.

In this section we introduce an interface problem involving a moving piston at one boundary and as a special case a classical tube problem with an interface and fixed boundaries.

2.1 Interface and piston problems.

We consider first a piston problem in which the tube contains two different gases separated by a contact discontinuity at some point $I(t) < L(t)$, where $I(t)$ and $L(t)$ represent the interface between the two gases and piston position respectively (see figure 1).

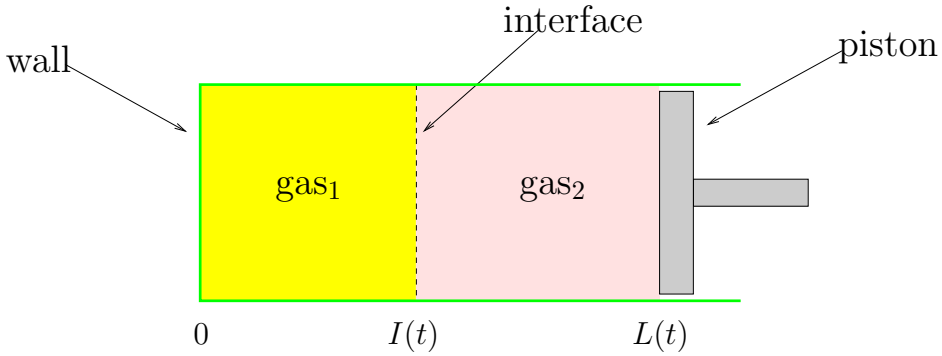

Figure 1: Physical setup for the piston problem

The governing equations are Euler equations of gas dynamics, that is

$$\frac{\partial \mathbf{q}}{\partial t} + \frac{\partial}{\partial x}\left[\mathbf{f}(\mathbf{q})\right] = \mathbf{0} \ , \tag{1}$$

with

$$\begin{aligned} \mathbf{q} &= [\rho, \rho u, E]^T \ , \\ \mathbf{f}(\mathbf{q}) &= [\rho u, \rho u^2 + p, (E+p)u]^T \ , \end{aligned} \tag{2}$$

and with the constitutive law for ideal gases

$$p = (\gamma(x,t) - 1)\left(E - \frac{1}{2}\rho u^2\right) \ , \tag{3}$$

where ρ, u, E, and p denote density, velocity, total energy density per unit volume, and pressure of the gas. The polytropic constant $\gamma(x,t)$ takes the value γ_1 on $0 \le x < I(t)$,

and γ_2 on $I(t) < x \leq L(t)$. The motion of the piston is driven by Newton's equation

$$\frac{d^2L}{dt^2} = \frac{A}{m}(p(L(t),t) - p_{out}(t)) \ , \tag{4}$$

where A is the area of the piston, m is its mass and $p_{out}(t)$ is the external pressure.

Next we consider the classical tube problem with an interface and fixed boundaries which is a particular case of the previous, obtained by setting $A = 0$.

2.2 Lagrangian formulation.

By introducing the Lagrangian coordinate ξ given by

$$\xi = \int_{x_0(t)}^{x} \rho(z,t)dz \ ,$$

where $x_0(t)$ denotes the Eulerian coordinate of the first fluid particle of the domain, the Euler equations (1)-(2) can be transformed in Lagrangian form

$$\frac{D\mathbf{q}}{Dt} + \frac{\partial}{\partial \xi}\left[\mathbf{f}(\mathbf{q})\right] = \mathbf{0} \ , \tag{5}$$

which is also in conservation form with

$$\begin{aligned} \mathbf{q} &= [V, u, \mathcal{E}]^T \ , \\ \mathbf{f}(\mathbf{q}) &= [-u, p, up]^T \ , \end{aligned} \tag{6}$$

here the time derivative is the Lagrangian derivative

$$D/Dt = \partial/\partial t + u\partial/\partial x \ ,$$

the new field variables are defined by $V(\xi,t) = \rho^{-1}, \mathcal{E} = E/\rho$, and the equation of state (3) becomes

$$p = (\gamma(\xi,t) - 1)\left(\mathcal{E} - \frac{1}{2}u^2\right)/V \ . \tag{7}$$

The inverse transformation of coordinate is

$$x = x_0(t) + \int_0^{\xi} V(z,t)dz \ , \tag{8}$$

and $x_0(t)$ satisfies the equation

$$\frac{d}{dt}x_0 = u(\xi = 0, t) \ .$$

In our case the left boundary is fixed, and therefore $x_0(t) \equiv 0$. Hence, $0 \leq \xi \leq \xi_{\max}$ will be our "computational domain" in which we have a fixed uniform grid with $\xi_j = (j - 1/2)\Delta\xi$ for $j = 1, 2, \ldots, J$ denoting the center of j-th cell, and $\Delta\xi = \xi_{\max}/J$.

2.2.1 Boundary conditions

We would like to spend a few words about the boundary conditions at the edges of the computational domain.

At the left edge, we use standard boundary conditions for a wall, namely

$$u = u_b, \quad \frac{\partial p}{\partial x} = 0, \quad \frac{\partial \rho}{\partial x} = 0 \tag{9}$$

where u_b denotes the wall velocity (in our case $u_b = 0$).

The condition on the velocity is obvious, since at the wall the gas has the same velocity of the boundary. The other two conditions can be deduced by a symmetry argument, by considering that a wall is equivalent to having a symmetric gas configuration on the other side of it. This symmetry consideration no longer applies on the moving boundary, if the speed of the piston is not constant. In this case one has to resort to other conditions.

On the moving boundary, the velocity of the gas is equal to piston velocity. Direct compatibility of the boundary condition on the velocity with momentum conservation law, which is

$$\frac{Du}{Dt} + \frac{\partial p}{\partial \xi} = 0,$$

gives

$$\frac{\partial p}{\partial \xi} = -\frac{d^2 L}{dt^2}. \tag{10}$$

The condition on the density can be obtained by assuming that, because the piston is adiabatic, the entropy at the piston is flat, i.e. $\partial S/\partial x = 0$. This condition, expressed in Eulerian coordinates, becomes

$$\frac{\partial \rho}{\partial x} = \frac{1}{c_s^2}\frac{\partial p}{\partial x},$$

where $c_s^2 = (\partial p/\partial \rho)_S$ is the square of the sound speed. In Lagrangian coordinates, this relation reads

$$\left.\frac{\partial p}{\partial V}\right|_S \frac{\partial V}{\partial \xi} = \frac{\partial p}{\partial \xi}, \tag{11}$$

where $-(\partial p/\partial V)_S$ is the square of the sound speed in Lagrangian coordinates.

Remark The numerical boundary conditions can be obtained by discretizing the above relations (10–11) at the boundaries. Using flat conditions of the form (9) instead of (10–11) for pressure and density also at the piston boundary produces an error which is first order in the space step, therefore the scheme is still consistent to the equations, but the accuracy is degraded.

3 Staggered central discretization.

3.1 The Nessyahu and Tadmor central scheme.

The Nessyahu and Tadmor central scheme [15] has the form of a predictor-corrector scheme

$$\begin{aligned}
\mathbf{q}_j^{n+1/2} &= \mathbf{q}_j^n - \frac{\mu}{2}\mathbf{f}'_j \ , \\
\mathbf{q}_{j+1/2}^{n+1} &= \frac{1}{2}(\mathbf{q}_j^n + \mathbf{q}_{j+1}^n) + \frac{1}{8}(\mathbf{q}'_j - \mathbf{q}'_{j+1}) - \mu\left(\mathbf{f}\left(\mathbf{q}_{j+1}^{n+1/2}\right) - \mathbf{f}\left(\mathbf{q}_j^{n+1/2}\right)\right) \ ,
\end{aligned}$$

where $\mathbf{q}_j^n$ denotes an approximation of the cell average of the field at time t_n

$$\mathbf{q}_j^n \approx \frac{1}{\Delta\xi}\int_{\xi_j-\Delta\xi/2}^{\xi_j+\Delta\xi/2} \mathbf{q}(\xi, t_n)\, d\xi \ ,$$

$\mu = \Delta t/\Delta\xi$ and $\mathbf{q}'_j/\Delta\xi$ and $\mathbf{f}'_j/\Delta\xi$ are a first order approximation of the space derivatives of the field and of the flux and can be computed in several ways. The simplest choice is

$$\begin{aligned}
\mathbf{q}'_j &= \mathrm{MM}(\mathbf{q}_{j+1} - \mathbf{q}_j, \mathbf{q}_j - \mathbf{q}_{j-1}) \ , \\
\mathbf{f}'_j &= \mathrm{MM}(\mathbf{f}_{j+1} - \mathbf{f}_j, \mathbf{f}_j - \mathbf{f}_{j-1}) \ ,
\end{aligned}$$

where $\mathrm{MM}(v, w)$ is the min-mod limiter

$$\mathrm{MM}(v,w) = \begin{cases} \mathrm{sgn}(v)\cdot\min(|v|,|w|) & \text{if } \mathrm{sgn}(v) = \mathrm{sgn}(w) \\ 0 & \text{otherwise .} \end{cases}$$

This limiter, however, may cause a degradation of accuracy near local extrema (clipping phenomena). In order to avoid this effect we use the UNO limiter proposed by Harten [11]

$$w'_j = \mathrm{MM}(d_{j-1/2} + \frac{1}{2}\mathrm{MM}(D_{j-1}, D_j), d_{j+1/2} - \frac{1}{2}\mathrm{MM}(D_j, D_{j+1})) \ , \tag{12}$$

where

$$d_{j+1/2} = \bar{w}_{j+1} - \bar{w}_j, \quad D_j = \bar{w}_{j+1} - 2\bar{w}_j + \bar{w}_{j-1} \ .$$

Several other choices of the limiters are possible, as discussed in [15].

The time step Δt must satisfy the stability condition

$$\mu \max_j \rho(A(\mathbf{q}_j^n)) \leq \frac{1}{2} \ ,$$

where $\rho(A)$ denotes the spectral radius of the Jacobian matrix

$$A = \left[\frac{\partial f_i}{\partial q_k}\right] \ .$$

This condition ensures that the generalized Riemann problems with piece-wise smooth data at time t_n do not interact during the time step Δt.

We note that after one time step, the numerical solution is computed on a staggered grid (see figure 2). After two time steps the numerical solution is evaluated on the original grid.

Remark For piston problems it is important to use a variable time step, chosen close to the limit of the CFL stability condition,

$$\Delta t^n = c\frac{\Delta \xi}{\max_j \lambda_j^n}$$

where c is the Courant number, $\lambda_j^n = \sqrt{\gamma_j^n p_j^n / V_j^n}$ denotes the sound speed at the j-th cell and time t^n, and $c \leq 1/2$ for stability reasons. Because of the compression of the system, the sound speed can change of an order of magnitude, and if an optimal time step is not used then the scheme becomes inefficient and inaccurate.

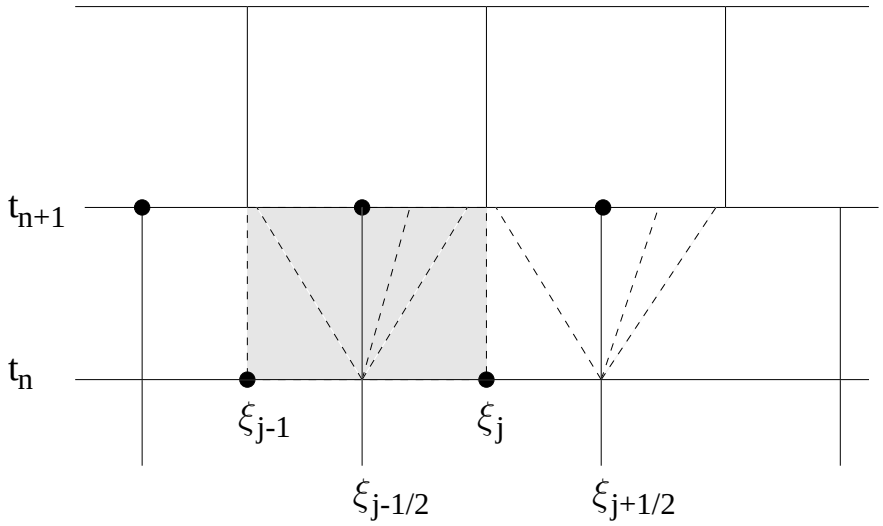

Figure 2: Staggered grid in space-time used in the NT scheme

3.2 Is second order really second order?

In this section we discuss some implementation details which are important to guarantee that the Lagrangian scheme for the piston problem is effectively second order in space and time.

a) Initial conditions.

In general, initial data are given in the Eulerian coordinates:

$$\begin{aligned} \rho(x,0) &= \rho_0(x) \\ p(x,0) &= p_0(x) \\ u(x,0) &= u_0(x) \ , \end{aligned} \tag{13}$$

for $x \in [0, L(0)]$.

Given the data (13) one first computes the maximum Lagrangian coordinate

$$\xi_{max} = \int_{x_0(t)}^{L(0)} \rho_0(z) dz \ ,$$

with a quadrature formula which is at list second order accurate. Then one defines $\Delta\xi = \xi_{max}/J$, and computes the new grid in the Eulerian coordinates at initial time:

$$
\begin{aligned}
& x_{-1/2} = -\Delta\xi/2\rho_0(0) \\
& \text{for } j = 1, \ldots, J+1 \\
& \qquad V_j = 1/\rho_0(x_j) \\
& \qquad u_j = u_0(x_j) \\
& \qquad \mathcal{E}_j = u_j^2/2 + V_j p_0(x_j)/(\gamma - 1) \\
& \qquad x^* = x_j + V_j \Delta\xi \\
& \qquad V^* = 1/\rho_0(x^*) \\
& \qquad x_{j+1} = x_j + \Delta\xi(V_j + V^*)/2 \\
& \text{end}
\end{aligned}
$$

The correction in the computation of the Eulerian coordinates x_j ensures second order accuracy in the assignment of the initial data. Note that initial data are assigned also on the two ghost cells near the boundary, centered at x_0 and x_{J+1}.

b) Boundary conditions and piston motion.
Boundary conditions can be assigned either every time step or just at even time steps. In both cases, suitable values are defined on a number of ghost cells, that depends on the limiter which is used for the reconstruction of the derivatives. For example, in the case of the UNO limiter (12), three or five ghost cells are needed at even time steps, see figures 3–4. When boundary conditions are assigned at every time step, we compute the values of the field to three ghost cells at even times steps, and to two ghost cells at odd time steps (see figure 3).

The values of the field at the cell containing the piston at odd time step is obtained as a result of the computation. When boundary conditions are assigned at even time steps only, the field is assigned at five ghost cells, and from it, it is computed on two ghost cells at odd time steps. In both cases, the field values at ghost cells are obtained by discretization of the boundary conditions illustrated in section 2.2.1. More specifically, we assume that on the ghost cells the pressure profile is linear,

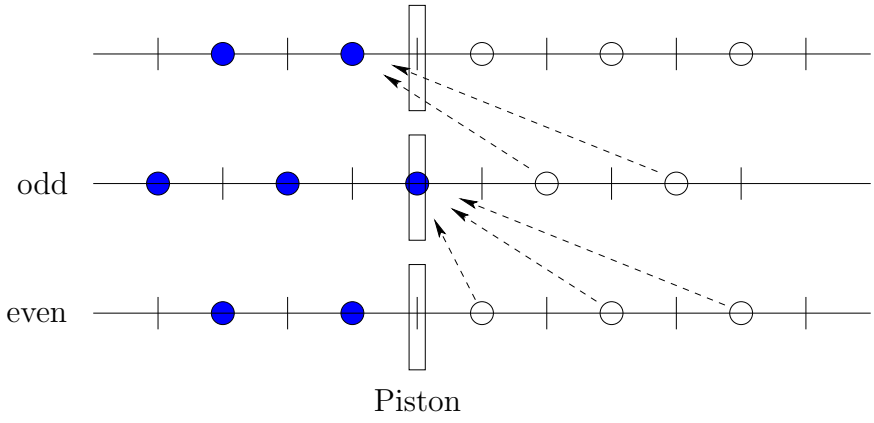

Figure 3: Three and two ghost cells (empty circles) are used at even and odd time steps, respectively. The field in the cell containing the piston at odd time step is computed in this way.

with a slope equal to the acceleration of the piston; the entropy is assumed to be constant, and the velocity relative to the piston is an odd function, in a frame of reference with the origin on the piston.

For even time steps, this discretization can be treated ad follows: the boundary condition for the pressure is discretized as

$$\frac{p^n_{J+1} - p^n_J}{\Delta\xi} = -a^n_p \tag{14}$$

where a is the piston acceleration, the subscript p indicates a value at the piston. From the piston equation of motion, to second order, we have

$$a^n_p = \frac{A}{m}\left(p_{out} - \frac{p^n_J + p^n_{J+1}}{2}\right). \tag{15}$$

Substituting (15) into (14) and solving for p_{J+1} one finds the pressure at the first ghost cell $J+1$. The pressure at the other two ghost cells is computed as

$$p^n_{J+2+k} = 2\,p^n_{J+1+k} - p^n_{J+k}\ , \qquad \text{for } k = 0, 1\ . \tag{16}$$

The specific volume V at the ghost cells is computed from the adiabaticity condition

$$V^n_{J+k} = V^n_J (p^n_{J+k}/p^n_J)^{(-1/\gamma)}\ , \qquad \text{for } k = 0, 1, 2\ . \tag{17}$$

The velocity at the ghost cells is computed from the equations

$$\frac{u^n_{J+1+k} + u^n_{J-k}}{2} = u^n_p \ , \qquad \text{for } k = 0, 1, 2 \ . \tag{18}$$

Analogous formulae hold for odd time steps n. The velocity of the piston, to second order, is computed by using trapezoidal rule

$$u^n_p = u^{n-1}_p + (a^n_p + a^{n-1}_p)\frac{\Delta t}{2}. \tag{19}$$

Naive boundary conditions are implemented by assuming a symmetric pressure and density distribution across the piston. For example, for even time steps, they are:

$$p^n_{J+1+k} = p^n_{J-k} \ , \quad V^n_{N+1} = V^n_N \ , \quad u^n_{J+1+k} = 2\, u^n_p - u^n_{J-k} \ , \quad \text{for} \quad k = 0, 1, 2 \ . \tag{20}$$

As we shall see, using such boundary conditions cause degradation of the accuracy.

When the boundary conditions on the ghost cells are assigned only at even time steps similar formulae can be derived by using the above assumptions. At the end of two time steps, after the field has been computed back on the original grid, two quantities have to be computed: the field at the five ghost cells (see figure 4) and the new velocity of the piston.

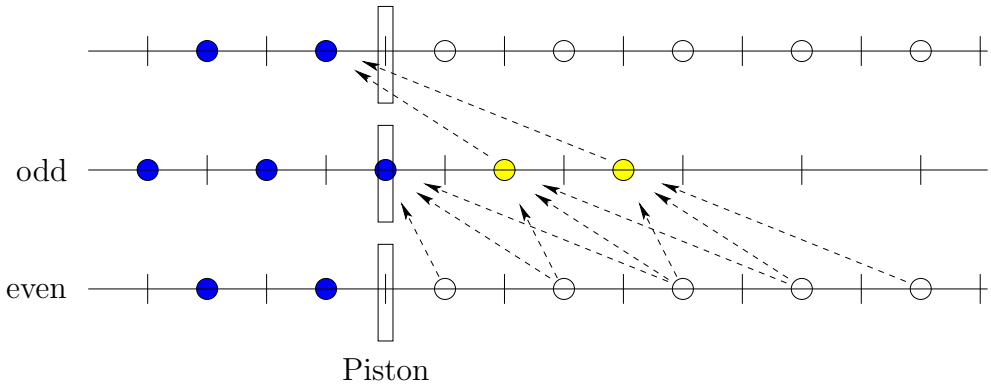

Figure 4: Five ghost cells (empty circles) are used at even time steps. The field in the cell containing the piston and two further ghost cells at odd time step are computed in this way.

3.3 One gas convergence test

Here we perform some convergence test to be sure that our scheme is effectively second order accurate. We consider a single gas, that is $\gamma = \gamma_1 = \gamma_2 = 1.4$, and compute the solution at two different times, namely $t = 0.7$ and $t = 10$, using $J = 50, 100, 200, 400, 800, 1600$ cells. The initial condition is a simple wave travelling with negative velocity

$$\begin{aligned} u(x,0) &= \begin{cases} 0 & \text{if} \quad |x-0.5| > \sigma \\ -\theta\sqrt{\gamma}\ \left(1+\cos\frac{\pi}{\sigma}(x-0.5)\right) & \text{otherwise ,} \end{cases} \\ \rho(x,0) &= \left(1+\frac{\gamma-1}{2\sqrt{\gamma}}\ u(x,0)\right)^{\frac{2}{\gamma-1}} \\ p(x,0) &= \rho(x,0)^{\gamma} \ , \end{aligned} \tag{21}$$

with $\theta = 0.02$ and $\sigma = 0.3$. The piston conditions are given by

$$L(0) = 1 \ , \qquad \frac{dL}{dt}(0) = 0 \ . \tag{22}$$

The remaining data are given by $A/m = 0.1$, $p_{out}(t) = 2$. UNO limiter (12) has been used in all numerical computation performed for this section.

The convergence results (L_1 norm of the error and accuracy order) are summarized in table 1.

J - $2J$	L_1 error and order in V		L_1 error and order in p	
50 - 100	5.7764082158E-05	1.754837990	7.7636250353E-05	1.786472917
100 - 200	1.7115869923E-05	1.736317277	2.2505188099E-05	1.730192423
200 - 400	5.1370693654E-06	1.515109181	6.7833284447E-06	1.546337247
400 - 800	1.7973063677E-06	1.902453661	2.3224638426E-06	1.899040341
800 - 1600	4.8075798986E-07		6.2270282797E-07	

Table 1: Convergence test at time $t = 0.7$, before the simple-wave wall-boundary interaction. Second order boundary condition at the piston.

Pressure profile for this test are shown in figure 5.

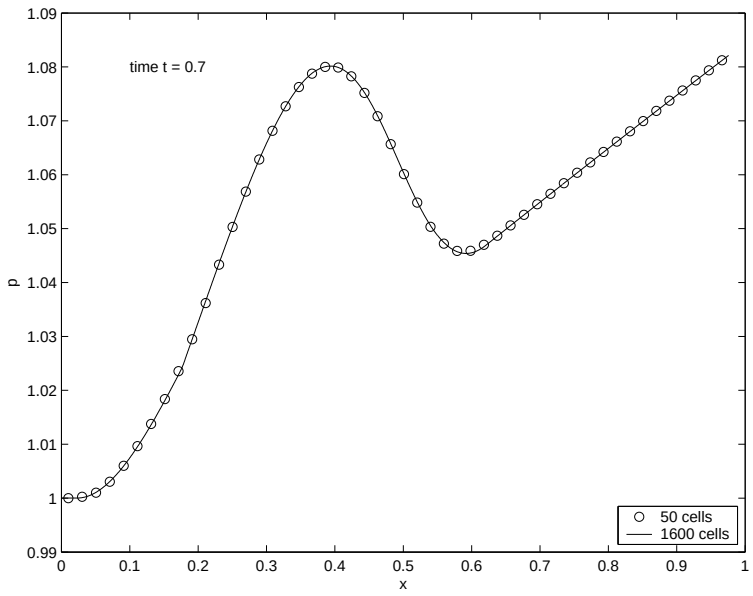

Figure 5: Pressure profile at time $t = 0.7$ for $J = 50$ circle and $J = 1600$ solid line. Second order boundary condition at the piston.

J - $2J$	L_1 error and order in V		L_1 error and order in p	
50 - 100	2.5297669345E-04	1.002327919	3.5982410191E-04	1.004176378
100 - 200	1.2628441618E-04	1.012790799	1.7939199461E-04	1.008157015
200 - 400	1.2998349848E-04	1.005194426	1.7726079386E-04	1.005086064
400 - 800	3.1179970392E-05	1.020296812	4.4438202167E-05	1.017017365
800 - 1600	1.5372190319E-05		2.1958554498E-05	

Table 2: Convergence test at time $t = 0.7$, before the simple-wave wall-boundary interaction. Naive boundary conditions at the piston.

The same test has been repeated, using naive boundary conditions at the piston, and the results are reported in table 2 and in figure 6.

In figure 7 we plot the time evolution of the pressure at the piston up to the time $t = 10$.

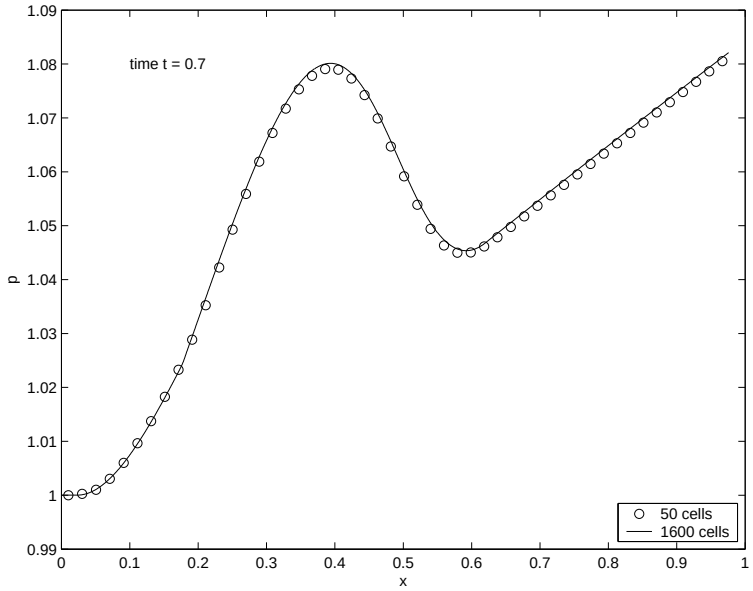

Figure 6: Pressure profile at time $t = 0.7$ for $J = 50$ circle and $J = 1600$ solid line. Naive boundary conditions at the piston.

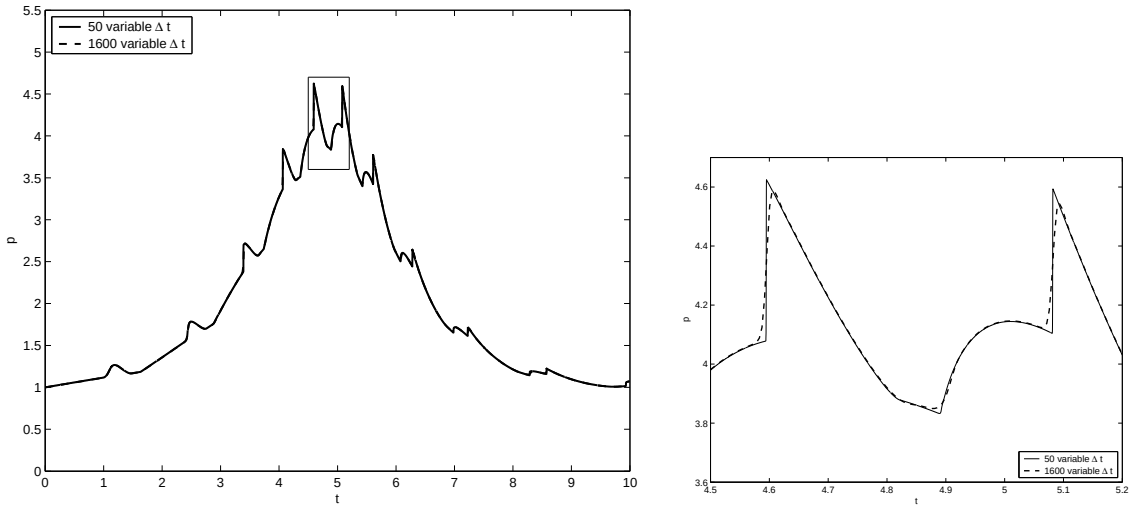

Figure 7: Pressure history at the piston for $J = 50$ solid line and $J = 1600$ dotted line. Left: Pressure evolution at the piston up to time $t = 10$. Right: zoom for the range $t \in [4.5, 5.2]$.

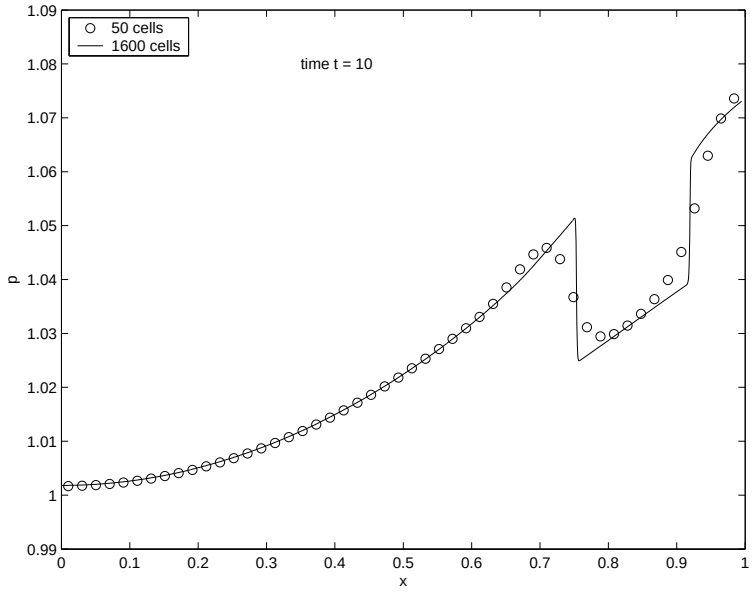

Figure 8: Pressure profile at time $t = 10$ for $J = 50$ circle and $J = 1600$ solid line. Second order boundary condition at the piston.

Figure 8 shows the space distribution of the pressure at time $t = 10$ with second order boundary condition at the piston. In figure 9 we plot the space distribution of the pressure at time $t = 10$ in the case of naive boundary condition at the piston.

As it is evident from the above tables and figures, our scheme gives the expected second order accuracy before interaction, and it gives more than first order accuracy (in L_1 norm) after a long time. Also, the use of the naive boundary conditions degrades the accuracy of the scheme. However, by comparing the reference solutions, namely the ones with 1600 cells, we can notice that in both cases convergence to the same reference solution is achieved as $\Delta x \to 0$.

The accuracy is degraded also if a first order scheme is used for the time evolution of the piston. The five point ghost cells treatment at the boundary has given similar results to the above treatment. We have not reported here the numerical results for the sake of brevity.

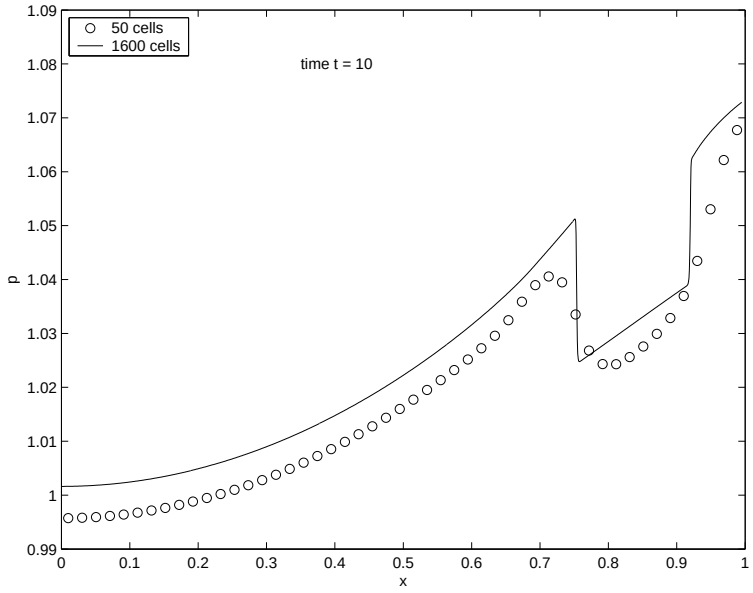

Figure 9: Pressure profile at time $t = 10$ for $J = 50$ circle and $J = 1600$ solid line. Naive boundary conditions at the piston.

3.4 Time step control

In many academic test cases the time steps for the computation is chosen to be a constant that satisfies the CFL condition. In the case of the piston, the CFL restriction may vary of several orders of magnitude during the evolution, therefore the use of a fixed time step is virtually and practically impossible. If one uses the smallest time step which guarantees stability in a whole piston chicle, then the scheme will be very inefficient and the numerical results will be very poor, due to the high numerical diffusion the central scheme possesses when the Courant number is far from its upper limit.

As an example, figure 10 shows a comparison of pressure profiles at time $t = 10$ obtained by using a fixed time step $\Delta t = 0.05/J$, chosen so that the most restricted CFL condition is satisfied, and an "optimal" time step

$$\Delta t^n = 0.45 \frac{\Delta \xi}{\max_j \lambda_j^n} \tag{23}$$

with $\lambda_j^n = \sqrt{\gamma p_j^n / V_j^n}$.

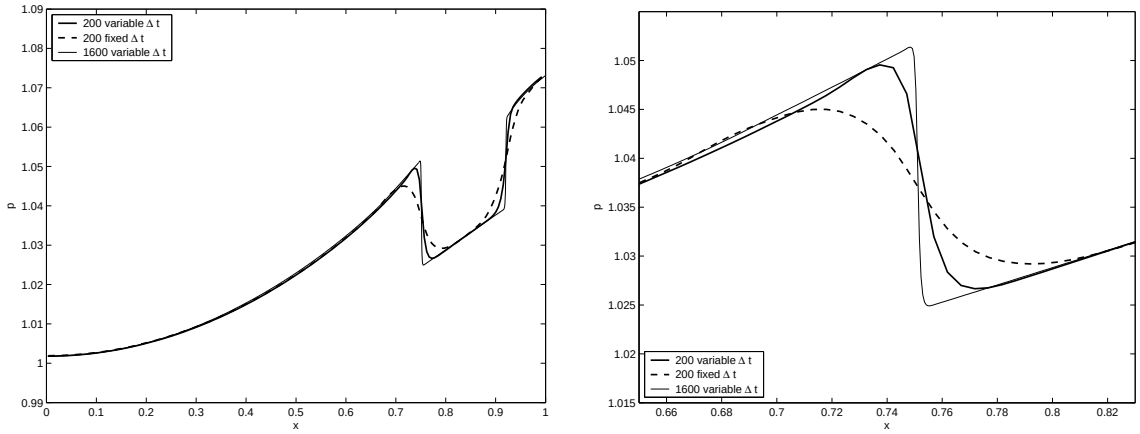

Figure 10: We compare the fixed Δt results marked by a dashed line, and the optimal step size results marked by a solid line. The sharp reference solution, with $J = 1600$ is also shown. Left: pressure profiles at time $t = 10$ for $J = 200$. Right: zoom at the first shock.

4 Balancing the pressure at the interface.

The development of this section starts from the observation that, due to the presence of the interface, several quantities (such as density and energy) may be discontinuous, but pressure and velocity have to be continuous across the interface. This condition is enforced in our scheme.

As stated above, being a material line, the interface moves with the velocities of the two gases (which are equal there). Using this condition, together with the jump relations across a discontinuity (also known as Rankine-Hugoniot conditions, see Whitham [17]) imposed at the interface we get that p does not jump at the interface, unless we take into account the effect of surface tension. On the other hand, we may suppose that there are two different gases across the interface, with different physical properties. In particular, the molecular mass of the two gases may be different, and in this case there would be a jump in the density, even if temperature and pressure are continuous.

We shall consider problems in which the interface is initially located exactly between two adjacent cells. This is obtained with a suitable choice of the grid. After one time step, the interface will be located in the middle of a cell (see figure 2 on page 9). The

field variables ($\rho, \rho u, E$ in Eulerian coordinates or $V, u, \mathcal{E}$ in Lagrangian coordinates) in the middle cell represent some average of the corresponding field variables on the two sides of the interface.

A key feature of the numerical scheme is that it should maintain static solutions. This means that if the initial data represents a static state, it should be unchanged after two time steps. This can be obtained by defining a suitable formula for the pressure of the interface cell, and by a suitable reconstruction of the field variables on the two sides of the interface.

At the initial time we assume that the interface is located at the boundary between cell j_w and cell $j_w + 1$. Because of the use of Lagrangian coordinates, the interface will always separate cell j_w from cell $j_w + 1$ at even time steps, and it will be in the middle of cell $j_w + 1/2$ at odd time steps (see figure 11 on page 21).

Let us denote by subscript 1 and 2 the values of the field variables on the two sides of the interface cell at odd time steps. The balance of the pressure on the two sides of the interface, $p_1 = p_2$, gives

$$\frac{\gamma_1 - 1}{V_1}\Big(\mathcal{E}_1 - \frac{1}{2}u^2\Big) = \frac{\gamma_2 - 1}{V_2}\Big(\mathcal{E}_2 - \frac{1}{2}u^2\Big) \ . \tag{24}$$

We assume that on the two sides of the interface there are two different gases, and we denote by η the ratio of the densities on the two sides

$$V_2 = \eta V_1 \ . \tag{25}$$

From perfect gas law, it follows that if the temperature is continuous across the interface, then η is given by the ratio of the molecular masses of the two gases. On the other hand, to assume the above condition is an approximation, which is reasonable only under certain circumstances but may not be appropriate in others or when a strong shock crosses an interface of two very different gases, it produces a jump in the temperature. This is not surprising, since Euler equations do not react to a temperature jump, because they are inviscid, and there is no heat conduction. We shall call this interface condition the *isothermal condition*.

In general, if we assume that the temperature ratio across the interface is constant in time, then η will be constant, and equal to the initial density ratio. In fact, from the

perfect gas law one has:

$$p_i = R_i \rho_i T_i, \quad i = 1, 2$$

where T denotes the absolute temperature, $R_i = R/m_i^*$ are the gas constant per unit mass, and m_1^* and m_2^* are the molecular weights of the two gases. From $p_1 = p_2$, it follows

$$\eta = \frac{\rho_1}{\rho_2} = \frac{T_2 m_1^*}{T_1 m_2^*} = \frac{V_2}{V_1} \ .$$

The cell average of the specific volume V and energy $\mathcal{E}$ at the interface cell $j_w + 1/2$ are

$$V = \frac{V_1 + V_2}{2}, \quad \mathcal{E} = \frac{\mathcal{E}_1 + \mathcal{E}_2}{2} \ . \tag{26}$$

Making use of above relations (24, 25, 26) we get the following formula for the pressure $p = p_1 = p_2$ in terms of the field variables at the interface

$$p(V, u, \mathcal{E}) = \frac{(1+\eta)(\gamma_1 - 1)(\gamma_2 - 1)}{\eta\gamma_1 + \gamma_2 - 1 - \eta} \left(\mathcal{E} - \frac{1}{2} u^2 \right) / V \ , \tag{27}$$

where in the isothermal condition

$$\eta = \frac{\rho_1(x_{j_w}, 0)}{\rho_2(x_{j_w}, 0)} = \frac{V_2(x_{j_w}, 0)}{V_1(x_{j_w}, 0)} \ .$$

Note that by setting $\eta = 1$ and $\gamma_1 = \gamma_2 = \gamma$ we recover from (27) the classical equation of state for a polytropic gas.

Once the interface quantities are known, the values of the field variables on the two sides can be computed

$$\begin{aligned} V_1 = \frac{2}{1+\eta} V \ , \quad \mathcal{E}_1 &= \frac{p(V, u, \mathcal{E}) V_1}{\gamma_1 - 1} + \frac{1}{2} u^2 \ , \\ V_2 = \frac{2\eta}{1+\eta} V \ , \quad \mathcal{E}_2 &= \frac{p(V, u, \mathcal{E}) V_2}{\gamma_2 - 1} + \frac{1}{2} u^2 \ . \end{aligned} \tag{28}$$

A better physical condition would be to impose that the interface is adiabatic. We impose this condition as follows. The ratio η is determined by imposing that the jump of the specific entropy S at the interface is constant in time. Let

$$S_i(t) = \frac{1}{\gamma_i - 1} \log \left(p V_i^{\gamma_i} \right) \ , \quad i = 1, 2$$

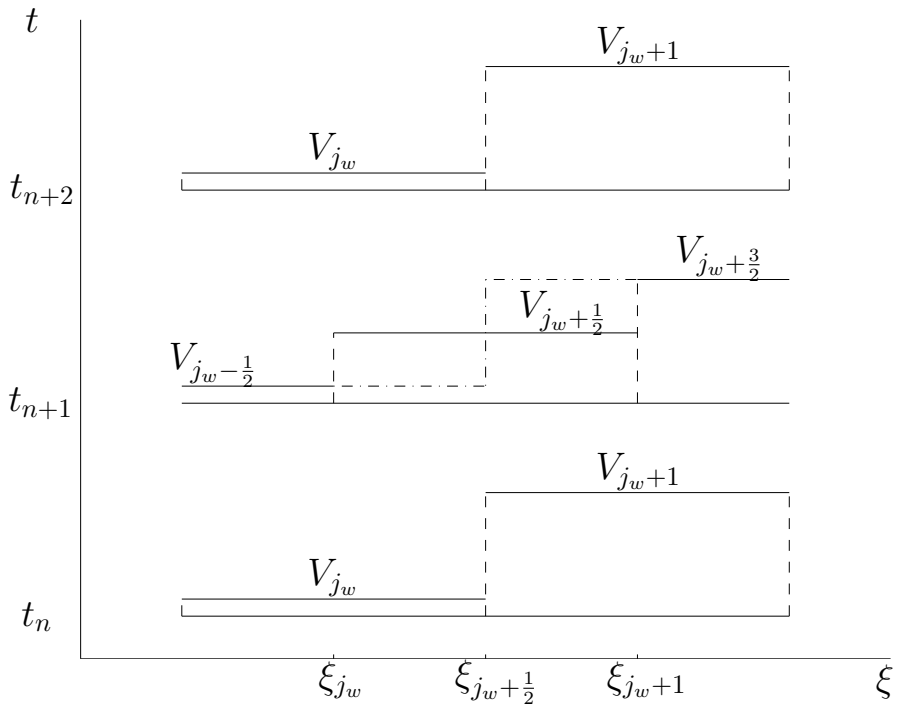

Figure 11: Evolution of the specific volume V near the interface cell for a steady solution. The results are obtained by our scheme.

denote the specific entropy on both sides of the interface. By imposing

$$S_1(t) - S_2(t) = S_1(0) - S_2(0) \ ,$$

and by making use of relations 27 and 28 we determine a nonlinear equation for η which is solved by Newton's iterations.

Figure 11 shows the evolution of the specific volume obtained by our scheme on two time steps for a steady solution. A similar picture is obtained for the evolution of the energy. Note how the scheme maintains static solutions.

5 Two gas numerical tests

In this section we report several numerical tests performed in order to validate the Lagrangian scheme.

All the quantities are represented using the more familiar Eulerian coordinate x rather than ξ. The Eulerian coordinate of the center of cell i (at even time steps) is obtained by a discrete version of Eq. (8),

$$x_k = x_0 + \Delta\xi \left(-\frac{1}{2} V_1 + \sum_{j=1}^{k} V_j \right) \ .$$

We used MinMod liniter (12) in all numerical test performed in this section.

5.1 Piston problem

The first model we consider is related to the physical setup of two gases separated by an interface between a solid wall and a plane piston (see figure 1 on page 4).

We perform three tests, with different values of γ. Two tests represents in fact a single fluid, with polytropic constant $\gamma_1 = \gamma_2 = 1.4$ and $\gamma_1 = \gamma_2 = 1.667$. In the third test there are two fluids with $\gamma_1 = 1.4$ and $\gamma_2 = 1.667$.

The related initial and interface conditions are as follows

$$\begin{gathered}
(\rho, u, p) = \begin{cases} (\rho_1, u_1, p_1) = (1.0, 0.0, 1.0) & 0 \le x \le I(0) \\ (\rho_2, u_2, p_2) = (1.0, 0.0, 1.0) & I(0) \le x \le L(0) \ , \end{cases} \\
I(0) = 0.5 \ , \quad L(0) = 1 \ , \quad \frac{dL}{dt}(0) = 0 \ , \\
\frac{dI}{dt}(t) = u_1(I(t), t) = u_2(I(t), t) \ ,
\end{gathered} \tag{29}$$

the remaining data are given by $A/m = 2$, $p_{out}(t) = 2$. For this test we applied the isothermal condition $\eta = 1$ at the interface.

Figure 12 illustrates a comparison of numerical results. We plot the evolution of the interface and the piston with time, in the three cases, obtained with two completely different methods. One is the central Lagrangian method described in this paper. The other is an upwind-based Eulerian scheme which adopts a moving grid approach, proposed by Fazio and LeVeque [7]. The agreement of the two approaches is remarkable, considering that only 100 grid points have been used.

In the initial condition the two gases are at rest, with constant pressure throughout the domain. The piston is set into motion by the (positive) difference between external and internal pressure.

Observe that the interface does not move for a while. It starts moving when the acoustic waves propagating inward from the piston reach it.

The motion of the system is oscillatory. As expected, the period of oscillation for the $\gamma = (1.4, 1.4)$ case is larger than the period for the $\gamma = (1.667, 1.667)$ case, because in the latter case the gas is stiffer and reacts more promptly to the pressure difference. The

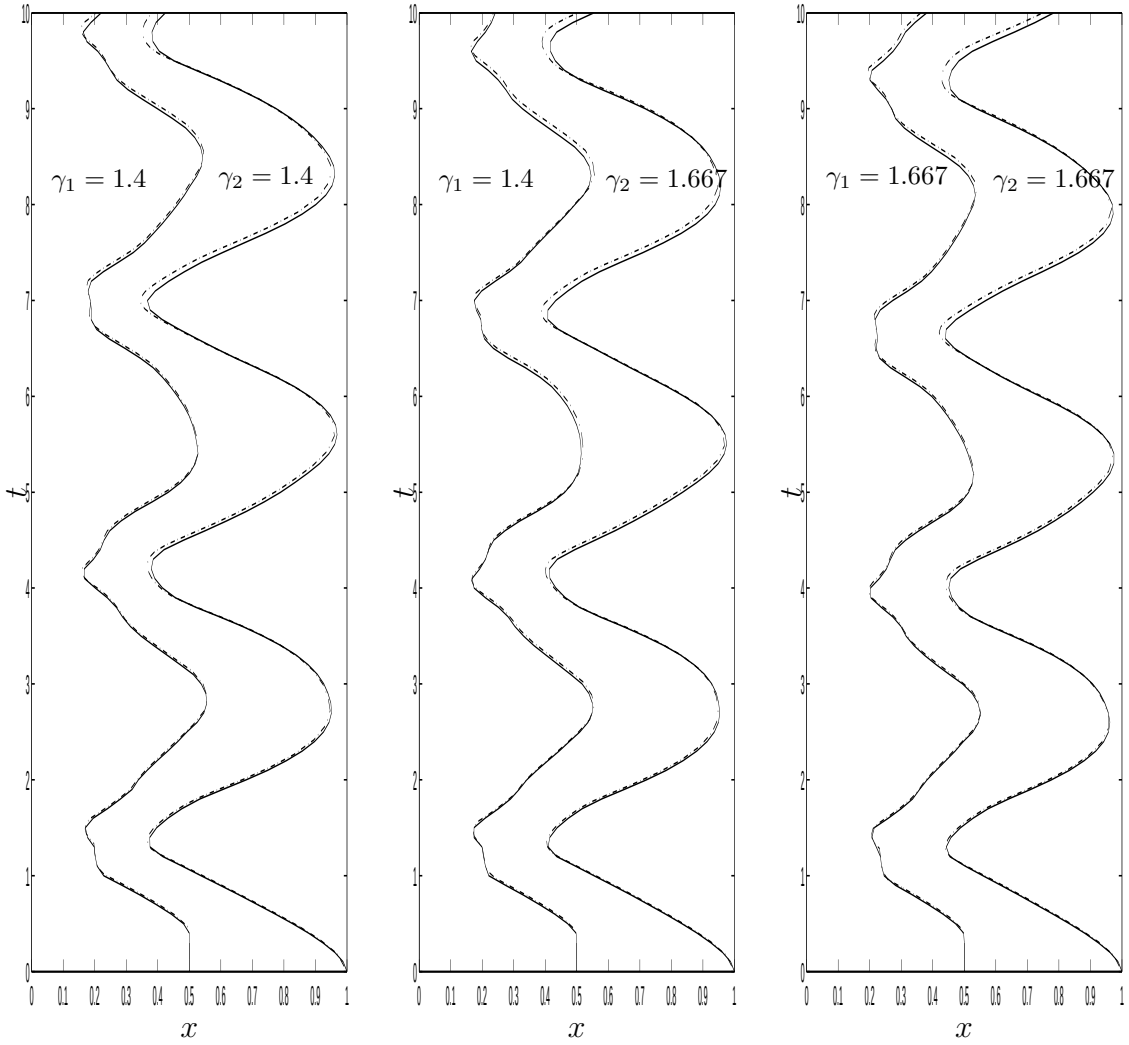

Figure 12: Numerical test for Eulerian and Lagrangian schemes: left $\gamma_1 = \gamma_2 = 1.4$, middle $\gamma_1 = 1.4, \gamma_2 = 1.667$ and right $\gamma_1 = \gamma_2 = 1.667$. Solid lines Eulerian scheme with 100 grid points. Dashed-dotted lines Lagrangian central scheme with 100 grid points.

behavior of the system with two gases, $\gamma_1 = 1.4$, $\gamma_2 = 1.667$, is intermediate between the previous two.

This is an academic example, which is used for the purpose of comparing two different numerical approaches. In a more realistic simulation one should use different densities for the initial condition of the two gases. However, in that case a comparison with the two single gas calculation can not be made.

5.2 Adiabatic approximation.

In this subsection we consider the adiabatic approximation for the piston problem of Section 1. In the adiabatic approximation the piston moves at a velocity which is much lower than the sound speed. As a result, for appropriate initial conditions, the pressure can be considered constant in the whole domain, and depends only on time. Furthermore, the entropies of both gases are constants, equal to their initial values. The above conditions alone are enough to describe the motion of the interface and of the piston by a single ordinary differential equation of second order. The above approximation is a good one for a sufficiently heavy piston.

The equation of motion can be obtained as follows. Because the motion is adiabatic, the evolution of the gas is isentropic, and the pressures of the two gases are given by

$$p_1 = k_1 \rho_1^{\gamma_1}, \quad p_2 = k_2 \rho_2^{\gamma_2}.$$

The densities of each gas are constant in space, and they are inversely proportional to the length of the corresponding region. We can therefore write

$$p_1 \tilde{k}_1 I^{-\gamma_1}, \quad p_2 \tilde{k}_2 (L - I)^{-\gamma_2}$$

where $\tilde{k}_1$ and $\tilde{k}_2$ are some constants that depend on the initial conditions.

By equating the pressures one can solve for L

$$L = I + c_1 I^{-\varrho} \tag{30}$$

where $\varrho = \gamma_1/\gamma_2$. The constant c_1 can be determined from the initial conditions

$$c_1 = (L_0 - I_0)(I_0)^{-\varrho}.$$

The equation of motion for the piston is

$$\frac{d^2L}{dt^2} = \frac{A}{m}(p(t) - p_{\text{out}}(t)) \ .$$

Differentiating Eq.(30), and using the relation for the pressure $p = p_0(I/I_0)^{\gamma_1}$, one obtains the following equation for I

$$\frac{d^2I}{dt^2}\left(1 + c_1\varrho I^{\varrho-1}\right) + c_1\varrho(\varrho-1)I^{\varrho-2}\left(\frac{dI}{dt}\right)^2 = \frac{A}{m}(c_2 I^{-\gamma_1} - p_{out}(t)) \ , \tag{31}$$

with $c_2 = p_0 I_0^{\gamma_1}$, and p_0 is the initial pressures on both sides of the interface. The piston position can be obtained from the interface position via the relation

$$L(t) = (L(0) - I(0))\left(\frac{I(t)}{I_0}\right)^{\varrho} + I(t) \ .$$

We solve Eq. (31) with the following data $L(0) = 1$, $p_0 = 1$, $A/m = 0.01, p_{out}(t) = 2, \gamma_1 = 1.4, \gamma_2 = 1.667$, and initial conditions

$$I(0) = 0.3 \ , \quad \frac{dI}{dt}(0) = 0 \ ,$$

and then we solve Eq. (5) with the same data and initial conditions

$$(\rho, u, p) = \begin{cases} (\rho_1, u_1, p_1) = (1.0, 0.0, 1.0) & 0 \le x \le I(0) \\ (\rho_2, u_2, p_2) = (1.0, 0.0, 1.0) & I(0) \le x \le L(0) \ . \end{cases}$$

The position of the interface is computed from the numerical solution by solving the equation

$$\frac{dI}{dt}(t) = u_1(I(t), t) = u_2(I(t), t) \ .$$

Figure 13 shows the good agreement between the adiabatic approximation and the numerical results obtained by our central scheme by setting $\Delta\xi = 0.005$, that is 200 mesh points. A Courant number $\mu \max_j \rho(A(\mathbf{q}_j^n)) = 0.45$ has been used.

Note that the average sound speed is around 2, so during the displayed time span the acoustic waves go back and forth between the piston and the wall more that 50 times.

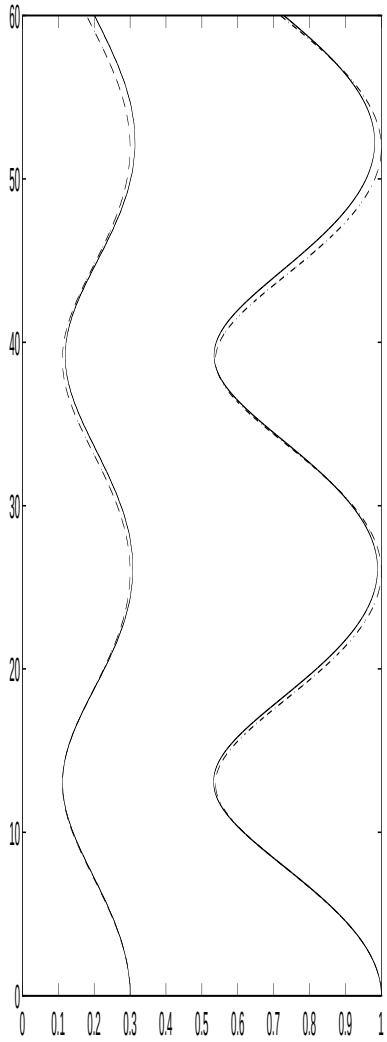

Figure 13: Adiabatic approximation: interface and piston positions in the $x - t$ plane, dashed line: adiabatic solution, solid line: numerical solution with 200 mesh-cells.

5.3 Shock-interface interaction

The physical setup for the test, as shown in figure 14, is to consider the interaction of a shock moving from left to right towards the interface. The tube is supposed to be open at both sided, and consequently inflow (outflow) boundary conditions at the left (right) boundary are provided.

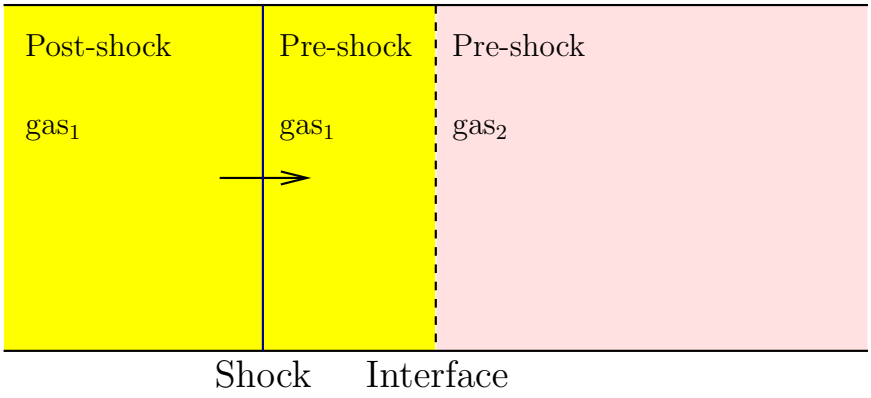

Figure 14: Physical setup for the shock-interface problems

The test problem considered here is the one studied by Abgrall and Karni [3]. They consider the following initial conditions (see [3], Test case 4).

$$\begin{aligned} (\rho_1, u_1, p_1) &= (1.0, 0.0, 500.0) \qquad 0 \le x < I(0) \\ (\rho_2, u_2, p_2) &= (1.0, 0.0, 0.2) \qquad I(0) < x \le L(0) \end{aligned} \tag{32}$$

with $I(0) = 0.5$, $L(0) = 1$,$\gamma_1 = 1.4$ and $\gamma_2 = 1.6$. At the interface, the ratio η is computed by using the adiabaticity condition, as illustrated in section 4.

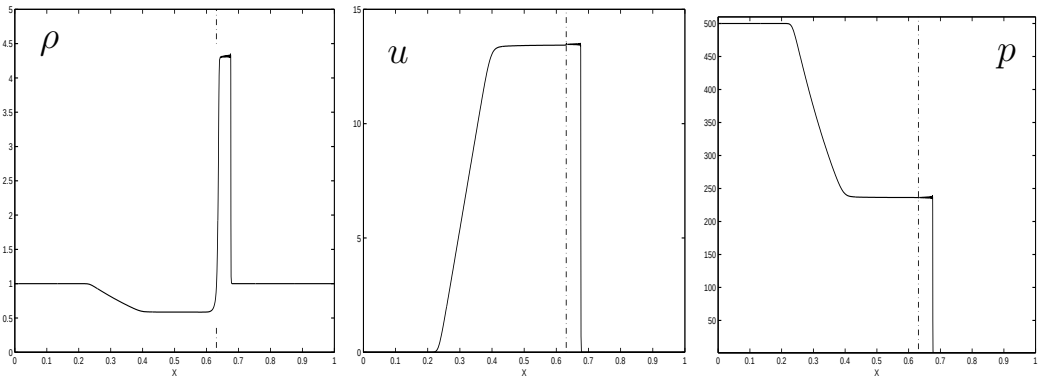

Figure 15: Abgrall-Karni Test 4 with 800 mesh cells. Left: density. Center: velocity. Right: pressure.

Figure 15 illustrates the numerical results for the shock-interface interaction problem. This can be compared with those reported in figure 6 of [3] where 800 grid points were

used. We notice that our results are free from the slight overshoots observed by those authors at the corner of the rarefaction fan. On the other hand, we can observe in figure 15 slight oscillations behind the shock location.

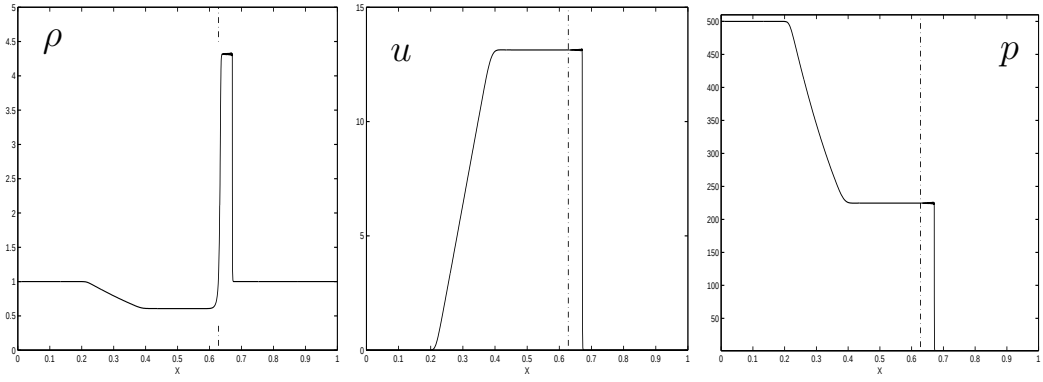

Figure 16: One fluid test with initial data (32)and 800 mesh cells, but with $\gamma = 1.6$. Left: density. Center: velocity. Right: pressure.

In figure 16 the calculation is repeated with a single gas with $\gamma = 1.6$. Note that the qualitative behavior of the two cases is very similar. The lack of resolution at the interface is not due to our treatment of the interface, but rather to the relatively poor performance of central schemes (with no artificial compression) at contact discontinuities, when compared to upwind schemes. The computations for this test have been performed with a Courant number 0.45.

6 Conclusions

In this paper we develop a staggered fully conservative central scheme for multi-fluid flows in Lagrangian coordinates. The central scheme does not require the solution to exact or approximate Riemann problems. Furthermore, by using Lagrangian coordinates, we do not require the use of additional equations for the interface motion, as is done, for example, with level set or mass fraction models. The main contribution is the derivation of a special equation of state to be imposed at the interface in order to avoid non-physical oscillations. For the piston problem we describe two different ways to impose boundary

conditions at the piston, that ensure second order convergence.

The proposed scheme is validated by solving several tests concerning one-dimensional hyperbolic interface problems. In particular we compare our results with: a moving mesh reference solution for a piston problem, a reference solution obtained by accurately solving a second order ordinary differential equation describing the equation of motion of the piston in the adiabatic approximation, and a benchmark shock-interface interaction problem. The agreement of the solutions obtained by the present method with those available in the literature shows the effectiveness of the proposed approach.

References

[1] R. Abgrall. Generalization of the Roe scheme for the computation of mixture of perfect gases. *Rech. Aérosp.*, 6:31–43, 1988.

[2] R. Abgrall. How to prevent pressure oscillations in multicomponent flow calculations: a quasi conservative approach. *J. Comput. Phys.*, 125:150–160, 1996.

[3] R. Abgrall and S. Karni. Computation of compressible multifluids. *J. Comput. Phys.*, 169:594–623, 2001.

[4] D. J. Benson. Computational methods in Lagrangian and Eulerian hydrocodes. *Comput. Methods Appl. Mech. Engrg.*, 99:235–394, 1992.

[5] S. F. Davis. An interface tracking method for hyperbolic systems of conservation laws. *Appl. Numer. Math.*, 10:447–472, 1992.

[6] R. Fazio. Comparison of two conservative schemes for hyperbolic interface problems. In F. Brezzi, A. Buffa, and A. Murli, editors, *Numerical Mathematics and Advanced Applications*, pages 85–93. Springer-Italia, Milano, 2003.

[7] R. Fazio and R. J. LeVeque. Moving-mesh methods for one-dimensional hyperbolic problems using CLAWPACK. *Comp. & Math. Appl.*, 45:273–398, 2003.

[8] R. Fazio and G. Russo. Eulerian and Lagrangian schemes for hyperbolic interface problems. In H. Freistühler and G. Warnecke, editors, *Intenational Series of Nu-*

merical Mathematics, volume Vol. 140, pages 347–356, 2001. Eighth International Conference on Hyperbolic Problems, Teory, Numerics, Applications, Magdeburg, 28 February - 3 March, 2000.

[9] R. Fedkiw and Xu-Dong Liu. The ghost fluid method for viscous flows. CAM Report n. 98-44, October 1998.

[10] R. P. Fedkiw, T. Aslam, B. Merriman, and S. Osher. A non-oscillatory eulerian approach to interfaces in multimaterial flows (the ghost fluid method). *J. Comput. Phys.*, 152:457–492, 1999.

[11] A. Harten, B. Engquist, S. Osher, and S. Chakravarthy. Uniformly high order accurate essentially non-oscillatory schemes iii. *J. Comput. Phys.*, 71:231–303, 1987.

[12] S. Karni. Hybrid multifluid algorithms. *SIAM J. Sci. Comput.*, 17:1019–1039, 1996.

[13] B. Larouturou. How to preserve the mass fraction positive when compressible multicomponent flows. *J. Comput. Phys.*, 95:59–84, 1991.

[14] W. Mulder, S. Osher, and J. Sethian. Computing interface motion: The compressible Rayleigh-Taylor and Kelvin-Helmholtz instabilities. *J. Comput. Phys.*, 100:209–228, 1992.

[15] H. Nessyahu and E. Tadmor. Non-oscillatory central differencing for hyperbolic conservation laws. *J. Comput. Phys.*, 87:408–463, 1990.

[16] H. Wang, M. Al-Lawatia, and R. C. Sharpley. A characterictic domain decomposition and space-time local refinement method for first-order linear hyperbolic equations with interfaces. *Numer. Meth. Partial Differential Equations*, 15:1–28, 1999.

[17] G. B. Whitham. *Linear and nonlinear waves*. Wiley, New York, 1974.